RSC Advances

ROYAL SOCIETY OF CHEMISTRY

www.rsc.org/advances

Journal Name

ARTICLE

Exploring the Low-lying Structures of $Au_n(CO)^+$ (n = 1-10): Adsorption and Stretching Frequencies of CO on Various Coordination Sites

Received 00th January 20xx,
Accepted 00th January 20xx

DOI: 10.1039/x0xx00000x

www.rsc.org/

Jie Wang[a, b, c], Qing-Bo Yan[b], Jun Ma[a], Xizi Cao[a], Xiaopeng Xing*[a] and Xuefeng Wang[a]

The low lying structures of $Au_n(CO)^+$ (n = 1-10) within 1.0 eV from their global minima were explored using a structure searching program (Atomic Global Minimum Locator) and density functional theory (DFT) calculations. According to general chemical intuitions, CO should prefer to stay on the lowest coordination sites of gold frames. However, our calculations showed that this preference becomes very weak in large $Au_n(CO)^+$, and even negligible for their compact three dimensional structures. This character relates to the intrinsic fluxionality of gold cluster frames, which apparently readjust their bond parameters after CO adsorption. The stretching frequency of a terminal-bonded CO decreases with increasing cluster size, and structural details of the adsorption sites have insignificant influences. The bridge-bonded COs, on the contrary, has far low stretching frequencies mainly determined by structural details of the two bridge sites. The frequency variation of CO relates to the electron donation and back-donation between gold and CO. Since all the above regularities on the adsorption and frequency of CO were summarized from large amount of low lying structures rather than some specific ones, they can be used to understand adsorption of CO on active sites of real gold catalysts, whose structures are diversiform and usually unclear.

Introduction

The catalytic properties of dispersed gold species in CO oxidization reactions were discovered about two decades ago.[1, 2] This finding has inspired enduring efforts to explore the structures and reactivity of small gold species. Model gold species were prepared on metal oxides and characterized using various surface techniques.[3-6] These experiments have shown the effects of clusters' sizes, charges, band gaps, and the defects of supporting substrates. However, the structural details of the active sites are usually unclear. Additionally, the fluxionality of small gold species has been noticed in various experimental and theoretical studies.[7-10] This character could make structures of gold sites diversiform and strongly dependent on the specific surroundings. This complexity makes it even more challenging to clearly understand interactions of CO with real gold catalyst at molecular level.

Naked gold clusters were generated in the gas phase and well characterized using different strategies. For example, the structures of Au_n^- were determined by combinations of theoretical calculations and various experiments including the ion mobility technique,[11] the photoelectron spectroscopy[12-14] and the trapped ion electron diffraction.[15-17] The structural information of Au_n^+ mainly comes from ion mobility measurement and theoretical calculations.[18-20] Experiments in the gas phase show that O_2 tends to be an electron acceptor while CO acts as an electron donor when they interact with gold clusters.[21-27] Consequently, CO prefer to stay on cationic gold sites, while O_2 tend to be activated by anionic gold species. The full catalytic circles of CO oxidation were observed on some gold clusters[22, 28] and theoretical works proposed many possible reaction mechanisms.[28-42] In spite of all those valuable clues from the gas phase studies, there are still many challenges to understand the real catalytic processes on surfaces. A significant one is that the lowest lying structures in gas phase are usually not what they are in real catalysts. An example is that Au_8 on an F-center of MgO, which has a different structure[43] from the lowest lying ones of the naked cationic, anionic or neutral Au_8.[11, 18, 44] In order to obtain more profound and accurate understanding on how real gold catalysts work, some general regularities applicable for various gold structures are of great meaning.

Reaction of Au_n^+ (n=1-65) with CO has been studied in the gas phase. Kinetic measurements obtained the bond energies of CO on different cluster sizes.[45] The subsequent work indicated that these bond energies are strongly dependent on the net positive charge around the adsorption sites.[25] The infrared photo dissociation spectra of saturated $Au_n(CO)_m^+$ (n = 1-10) gave the CO stretching frequencies around 2120-2180 cm^{-1}, and additionally showed a 3D to 2D transition of the gold frames during adsorption processes.[9] There have been many theoretical works on adsorptions of CO on cationic gold species.[9, 25, 36, 41, 42, 45-48] Most of these studies focused on predicting the global minima which possibly present in the gas phase experiments. The CO adsorptions on supported cationic gold species also attracted great attentions. The IR bands around 2150 cm^{-1} in surface studies have been empirically assigned to those on cationic gold sites,[4, 49, 50] which is slightly higher than those of COs on small neutral gold clusters (2050-2150 cm^{-1}).[51]

[a] Department of Chemistry, and Shanghai Key Lab of Chemical Assessment and Sustainability, Tongji University, 1239 Siping Road, Shanghai, 200092, China, E-mail: xingxp@tongji.edu.cn.
[b] College of Materials Science and Opto-Electronic Technology, University of Chinese Academy of Sciences, Beijing, 100049, China.
[c] CHINALCO Research Institute of Science and Technology, Southern District of Future Science & Technology Park, Beijing, 102209, China.

Electronic Supplementary Information (ESI) available: [All theoretical structures of $Au_n(CO)^+$ (n=6-10) within 1.0 eV energy range were summarized in supporting materials Figure S1-S5]. See DOI: 10.1039/x0xx00000x

In this work, we explored the low lying structures of $[Au_n(CO)]^+$ (n = 1-10) using a structure searching program (Atomic Global Minimum Locator) and density functional theory (DFT) calculations. Other than making great efforts to determine the global minimum of each size, we considered the characters and properties of a large amount of low lying structures within 1.0 eV energy range. This energy value is roughly the order of interacting energies between substrates and small metal species. Our results revealed some general regularities about CO adsorption and stretching frequency on different coordination sites of gold. The obtained conclusions should be useful to understand what happens on the active gold sites in real catalysts.

Calculation methods

All calculations were performed using the GAUSSIAN 09 suite package[52] and a structure searching program of Atomic Global Minimum Locator.[53] This searching program has been used to locate the lowest structures of metal clusters and organic complexes.[54-56] Firstly, we combined the simulated annealing algorithm method in Atomic Global Minimum Locator and the DFT method based on the hybrid Becke-Lee-Yang-Parr functional (B3LYP)[57, 58] in GAUSSIAN 09 to locate the low lying structures of $[Au_n(CO)]^+$ (n = 1-10). The B3LYP method has been shown to be reliable in predicting the structures of small gold species, evaluating the relative energies of different isomers, and calculating the stretching frequencies of CO adsorbed on gold.[25, 47, 59-65] In the structural searching processes, the lanl2dz basis set was used for Au and the 6-31G(d) basis set for C and O (level I). As supplementary to this first structural searching strategy, we manually designed structures by putting CO on each of the possible adsorption sites of all previously reported structures of $Au_n^{+/0/-}$,[11, 12, 18, 19, 66] and also optimized them at aforementioned level I. After removing the duplicated ones from these two structural locating strategies, the frequencies of all structural candidates were analyzed to make sure they are real minima. For $Au_n(CO)^+$ (n=1-5), the optimized structures from level I were further optimized using B3LYP method with larger basis sets, Aug-cc-PVTZ-pp for Au[67, 68] and Aug-cc-PVTZ for C and O (level II).[69, 70] The CO frequencies were calculated using analytic second derivatives at both level I and level II. For $Au_n(CO)^+$ (n=6-10), the single point energies of the optimized structures at level I were recalculated at level II and the CO frequencies were only calculated at level I.

Results and discussion

A. Large quantities of low lying structures of $Au_n(CO)^+$

For $Au_n(CO)^+$ (n=1-5), the optimization at both level I and level II got consistent structures and roughly same relative energies. The low lying structures from these two levels were displayed in Figure 1, which are sequenced according to the relative energies at level II. The determined global minima for Au_nCO^+ (n=1-6) are consistent with those reported in ref [45, 48]. The second lowest lying structures for both Au_2CO^+ and Au_3CO^+ contain a bridge-bonded CO, which are 0.6-0.8 eV and 1.5-1.6 eV higher than their global minima, respectively. For $Au_4(CO)^+$, the structures 2-5 are within 1.0 eV from its lowest lying structure 1, and the structure 5 contains a bridge-bonded CO. For $Au_5(CO)^+$, the structures 1-4 are within the 1.0 eV energy range, and their energy sequence is consistent with that in ref [45].

The isomer populations of $Au_n(CO)^+$ increase enormously from n=6. Since the results of Au_nCO^+ (n=1-5) indicate that further optimization at level II does not apparently change the structures from level I, $Au_n(CO)^+$ (n=6-10) were only optimized using level I and only the single point energies were recalculated at level II. All the structures of $Au_n(CO)^+$ (n=6-10) within 1.0 eV energy range were summarized in supporting materials Figure S1-S5. They were grouped as terminal adsorption complexes and bridge adsorption ones. Each group was sequenced separately according to the relative energies from level II. In Figure 2, we further classified the low lying structures of $Au_n(CO)^+$ (n=6-10) according to structural details of their adsorption sites. The nomenclature and the symbols of each type were shown in Figure 2a. The 2D-II, 2D-III and 2D-IV means that the adsorption happens on a two dimensional gold site, in which the gold atom bonding CO connects with 2, 3 and 4 other gold atoms, respectively. Similarly, the 3D-III, 3D-IV, 3D-V and 3D-VI means that the adsorption gold site is three dimensional and the gold atom bonding CO connecting with 3, 4, 5 and 6 other gold atoms, respectively. The bridge symbol means CO bridges on two gold atoms. The geometries of the three lowest lying ones for each type (if they are within the 1.0 eV energy range) were listed inside the figure panels. For $Au_6(CO)^+$, twenty low lying structures were shown in Figure S1 and Figure 2b. The structures 1-3 correspond to the three lowest lying ones predicted in ref [45], while their relative energies are slightly different. The forth structure of $Au_6(CO)^+$ reported in ref [45] is not a real minimum at two theoretical levels in this work. There are fourteen low lying structures of $Au_7(CO)^+$ in Figure S2 and Figure 2c. The structures 1-4 correspond to the four lowest lying ones in ref [45], and there are only a small differences on the structural details and energy intervals. For $Au_8(CO)^+$, forty seven isomers were located and shown in Figure S3 and Figure 2 d. The three lowest lying ones 1-3 are same as those reported in ref [45], while the forth lowest lying structure of $Au_8(CO)^+$ in ref [45] corresponds to the structure 11 of this work. The two lowest lying structures 1 and 2 of $Au_8(CO)^+$ are predicted to be planar even that of naked Au_8^+ were determined to be three dimensional. For $Au_9(CO)^+$, there are thirty two structures listed in Figure S4 and Figure 2e. Structures 1 and 4 correspond to the lowest lying Au_9^+ structure with CO adsorbed on different sites. For $Au_{10}(CO)^+$, there are totally eighty five structures displayed in Figure S5 and Figure 2f. Structures 1-5 are within 0.1 eV and the ones 1-3 correspond to the lowest lying Au_{10}^+ structure with CO on different adsorption sites.

B. A weak preference of CO on the lowest coordination sites

According to Figure 1 and 2, most of the global minima of $Au_n(CO)^+$ have the CO on their lowest coordination sites, which means the terminal gold atom for n =1 and 2 and the 2D-II type (shown in Figure 2a) for n = 3, 5, 6, and 8-10. This is consistent with the general chemical intuitions that CO tend to be adsorbed on the lowest coordination site of metals. However, when we considered all low lying isomers of $Au_n(CO)^+$ within 1.0 eV from the global minimum, we found that the ratio of the structures with CO on high coordination sites increases noticeably with the increase of cluster sizes. For $Au_{10}(CO)^+$, the isomer populations belonging to 2D-II, 3D-III and 3D-IV types are nearly equal. Even the bridge type of $Au_{10}(CO)^+$ have 6 isomers and the lowest lying one is only 0.2 eV higher than the global minimum. The energy levels are quite close for the low-lying structures of $Au_n(CO)^+$ (n=1-10) in this report and those of $Au_n(CO)^+$ (n=1-6) in previous reports[45, 48] with CO on different coordination sites. According to this observation, we can say there is indeed a preference of CO on the lowest coordination site on small gold clusters, however this preference becomes weak when cluster size increases. We found this argument is especially true for the compact three dimensional structures, as shown by the representative examples in Figure 3. The three structures of $Au_8(CO)^+$ (11, 12 and 13 from Figure S3) correspond to the lowest

lying 3D structure of Au_8^{+}[18] with CO on the different sites, and their energy differences are within 0.05 eV. Similarly, the structures of $Au_9(CO)^+$ (1 and 4 from Figure S4) correspond the global minimum of Au_9^{+}[18] with CO on its different sites, and their energy difference is 0.07 eV; the three structures of $Au_{10}(CO)^+$ (1, 2 and 3 from Figure S5) correspond to CO adsorption on different sites of the global minimum of Au_{10}^+,[18] and their energy differences are within 0.08 eV. In a previous theoretical studies, CO was put on all possible sites of Au_{21}^+ and the bond energies are shown dramatically different.[25] The physical origin of that large differences were attributed to different positive charges on various adsorption sites. We noticed that the gold frame was fixed in that calculation, therefore the results show a clear relation between the bonding energies and the positive charge of various sites. In this work, every structures were fully relaxed and optimized after CO was added, and we saw apparent readjustment of the bond parameters of the gold frames. Combining the figures revealed in ref [25] and this work, we can say that the net positive charges on individual cite indeed play an important role for adsorbing CO, while a small 3D gold cluster can adjust its frame, arriving structures with nearly same energies even the CO is initially put on its different sites. This character can be attributed to the intrinsic fluxionality of gold, which has been considered as one of the physical origins for their catalytic properties.

C. Calculating the stretching frequencies of COs in various structures

We calculated the CO stretching frequencies of all structures of $Au_n(CO)^+$ (n = 1 - 5) in Figure 1 using both level I and level II theories. Two scaling factors, 0.9703 and 0.9710, were obtained when dividing the experimental frequency (2143cm^{-1}) of a free CO molecule by the two calculated ones, 2208.6 cm^{-1} and 2207.1 cm^{-1}, at level I and level II, respectively. We also tested these two theoretical levels by calculating the CO frequency in $Au_3(CO)_3^+$, and got the scaled frequencies of 2187 cm^{-1} and 2178 cm^{-1}, respectively. Both of them are reasonably consistent with the experiment one (2182 cm^{-1}) in ref [9]. Table 1 lists the calculated CO stretching frequencies in $Au_n(CO)^+$ (n = 1 - 5). Those of the terminal-bonded CO at level I are slightly higher than those at level II. The differences are within 15 cm^{-1}. The values of $AuCO^+$ in table 1 (2237 cm^{-1} and 2234 cm^{-1}) are also very close to that (~2250 cm^{-1}) predicted using CCSD methods.[71] For most of the bridge-bonded COs, the stretching frequencies from the two levels are also very close. The only exception is the structure 5 of $Au_4(CO)^+$ (See Figure 1 and Table 1). The difference between CO frequencies from these two levels is about 50 cm^{-1}. However, the frequency sequences from two levels are always consistent. For $Au_n(CO)^+$ (n = 6 - 10), we only used level I calculating their CO stretching frequencies. In order to make a systematical comparison, Figure 4 lists all CO frequencies of $Au_n(CO)^+$ (n = 1-10) from level I. The structures were classified according to the type of the adsorption sites, same as what has been done in Figure 2. The new dash symbol ' - ' for $Au_n(CO)^+$ (n = 1, 2 and 4) stands for the structures where CO bonds on a terminal gold atom.

D. Dependence of CO stretching frequencies on the adsorption sites

In Figure 4, the frequencies of all terminal-bonded COs are higher than that of a free CO. This blue shift has been observed in various cationic gold carbonyls, such as $Au_n(CO)_m^+$ in the gas phase and $Au^{\delta+}$ on oxide surfaces.[4, 9, 49, 71, 72] The σ orbital of CO has partially anti-bonding characters, and the polarization of this orbital toward cationic gold species leads to an enhancement of the C-O bonding, and therefore the blue shift of the CO stretching frequency. With increasing cluster size, the positive charge is diluted and the pulling of CO σ orbital by gold sites decreases, making the blue shift decreases. For various isomers of $Au_n(CO)^+$ (n = 4-8), there is an unapparent trend that the CO frequency decreases with increasing coordination number of the adsorption site, and this trend nearly disappears for $Au_{9,10}(CO)^+$. Generally, bridge-bonded COs have lower frequencies than those of terminal-bond ones.[51] In Figure 4, the frequencies of bridge-bonded COs expand from lower than 1900 cm^{-1} to around 2100 cm^{-1}. These values seem independent on the cluster sizes, while strongly dependent on the structural details of the bridge sites. For example, the CO bridging on the planar structures in $Au_4(CO)^+$-6, $Au_5(CO)^+$-5, $Au_6(CO)^+$-19, $Au_7(CO)^+$-14, $Au_8(CO)^+$-47, $Au_9(CO)^+$-31, $Au_9(CO)^+$-32 or $Au_{10}(CO)^+$-82 has frequencies around 2050 cm^{-1}; the CO bridging on a terminal gold atom and another one belonging to any other type, like that in $Au_2(CO)^+$-2, $Au_3(CO)^+$-2, $Au_4(CO)^+$-5, $Au_6(CO)^+$-20 or $Au_{10}(CO)^+$-85 has frequencies around 1950 cm^{-1}; the CO bridging on three dimensional sites of gold has frequencies around 1900 cm^{-1}, like those in $Au_{10}(CO)^+$-80, 81 and 83. The diluting of positive charges along with increasing cluster size does not have significant effects on the frequencies of these bridge-bonded COs.

Usually, the stretching frequencies of adsorbed COs are closely related to the electron donation to and back-donation from metal moieties. We analyzed the frontier molecular orbitals in three representative structures $Au_{10}(CO)^+$-80, 82 and 1, which have a bridge CO on 3D sites (Figure 5a), a bridge CO on 2D sites (Figure 5b) and a terminal-bonded CO on a 2D-II site (Figure 5c), respectively. The HOMO orbitals in Figure 5a and 5b indicate electron back donation from the gold moieties to the π* of CO, and therefore lead to red-shifts of the CO stretching frequency. Qualitatively, the back donation in the structure of Figure 5a is more significant than that of Figure 5b, which leads to the lowest vibration frequency of CO bridging on 3D sites. The HOMO in Figure 5c comes mainly from gold moiety and no back donation exists in this case. The HOMO-1 in Figure 5c correspond to polarization of the σ orbital of CO (partially anti-bonding) toward the gold, causing the apparent blue-shift relative to that of a free CO.

Conclusions

We systematically searched the low lying structures of $Au_n(CO)^+$ (n = 1-10) using Atomic Global Minimum Locator and DFT calculations. Using the large amount of structures as model systems, we summarized some general regularities on CO adsorption and stretching frequencies on various coordination sites of gold species. Firstly, the preference of CO staying on the lowest coordination sites decreases with increasing cluster size. For the compact 3D gold frames of Au_8^+, Au_9^+, and Au_{10}^+, the structures with CO on different coordination sites have nearly degenerated energies. The frequencies of terminal-bonded COs decrease with increasing cluster sizes and diluting of positive charge. There is a very weak dependence of these CO frequencies on the structural details. Those of bridge-bonded COs, on the contrary, are mainly determined by the structures of their two bridging sites. Those bridging on 3D gold sites have apparently lower frequencies than those on 2D or dangling gold atoms. The weak preference of CO on certain coordination sites and the variation trend of CO stretching frequencies were well rationalized using the intrinsic fluxionality of gold and the electron transfer mechanism, respectively. Usually, the structural details of real catalysts are diversiform and unknown. The above regularities from large amount of various gold structures

should be applicable for understanding adsorption of COs on cationic gold sites in real catalysts.

Acknowledgments

This work was supported by the National Natural Science Foundation of China (Grant No. 21103226 and 21273278), the Fundamental Research Funds for the Central Universities, and Science & Technology Commission of Shanghai Municipality (14DZ2261100). The calculations were carried out on the Deepcomp7000 of Supercomputing Center, Computer Network Information Center of Chinese Academy of Sciences, and the computing server in Department of Chemistry, Tongji University.

Figure Captions

Figure 1
The theoretical low lying structures of $Au_n(CO)^+$ (n=1-5). Their electronic states and geometries are indicated. The numbers inside and outside of the parentheses indicate the relative energies from level I and level II, respectively. Level I: B3LYP method with lanl2dz basis set for Au and 6-31G(d) basis sets for C and O. Level II: B3LYP method with Aug-cc-PVTZ-PP basis set for Au and Aug-cc-PVTZ basis sets for C and O.

Figure 2
The theoretical low lying structures of $Au_n(CO)^+$ (n=6-10). The structures were optimized at level I and their relative energies were recalculated at level II. All the structures are classified according to the geometries of CO adsorption sites. The classification and the nomenclature are shown in (a). The results of $Au_n(CO)^+$ (n=6-10) are shown in (b)-(f), respectively. In each panel of (b)-(f), the horizontal axis stands for different types of adsorption sites and the vertical axis stands for the relative energy. The three lowest structures for each type of adsorption site (if there are) are displayed. The structures of each size are sequenced and numbered according to their relative energies at level II, which were included in supporting materials Figure S1-S5.

Figure 3
The representative structures of $Au_n(CO)^+$ (n=8-10), in which the gold moieties are compact three dimensional with CO on various adsorption sites. Their electronic states and geometries are indicated. The numbers inside and outside of the parentheses indicate their energies relative to the global minimum from level I and level II, respectively. The series numbers for these structures come from supporting materials Figure S3-S5.

Figure 4
The stretching frequencies of CO in low lying structures of $Au_n(CO)^+$ (n=1-10) (at level I). The classification and the nomenclature of these structure are same as that in Figure 2(a). The dash symbol '-' indicates CO on a terminal gold atom. The horizontal dashed line indicates the stretching frequency of a free CO molecule. The structures with a bridge-bonded CO are displayed and their series numbers come from supporting material Figure S1-S5.

Figure 5
The frontier molecular orbitals (at level I) of three representative structures of $Au_{10}(CO)^+$, which have a bridge-bonded CO on two 3D sites (a), a bridge-bonded CO on two 2D sites (b) and a terminal-bonded CO on the lowest coordination site (c), respectively.

Table 1
Theoretical frequencies of the low lying structures of $Au_n(CO)^+$ (n=1-5) in Figure 1. Level I: B3LYP method with lanl2dz basis set for Au and 6-31G(d) basis sets for C and O. Level II: B3LYP method with Aug-cc-PVTZ-PP basis set for Au and Aug-cc-PVTZ basis sets for C and O.

Structures		CO stretching frequencies (cm^{-1})	
		Level I	Level II
$Au(CO)^+$		2237	2234
$Au_2(CO)^+$	1	2215	2206
	2	1918	1935
$Au_3(CO)^+$	1	2198	2189
	2	1994	2000
$Au_4(CO)^+$	1	2186	2173
	2	2188	2174
	3	2193	2181
	4	2190	2179
	5	1948	2000
	6	2025	2019
$Au_5(CO)^+$	1	2183	2169
	2	2183	2170
	3	2171	2160
	4	2188	2176
	5	2018	2010

Notes and references

1. M. Haruta, T. Kobayashi, H. Sano and N. Yamada, *Chem. Lett.*, 1987, 405-408.
2. M. Haruta, N. Yamada, T. Kobayashi and S. Iijima, *J. Catal.*, 1989, **115**, 301-309.
3. M. Valden, X. Lai and D. W. Goodman, *Science*, 1998, **281**, 1647-1650.
4. Y. Hao, M. Mihaylov, E. Ivanova, K. Hadjiivanov, H. Knozinger and B. C. Gates, *J. Catal.*, 2009, **261**, 137-149.
5. J. C. Fierro-Gonzalez, J. Guzman and B. C. Gates, *Top. Catal.*, 2007, **44**, 103-114.
6. A. Sanchez, S. Abbet, U. Heiz, W. D. Schneider, H. Hakkinen, R. N. Barnett and U. Landman, *J. Phys. Chem. A*, 1999, **103**, 9573-9578.
7. H. Hakkinen, W. Abbet, A. Sanchez, U. Heiz and U. Landman, *Angew. Chem. Int. Ed.*, 2003, **42**, 1297-1300.
8. H.-J. Zhai, L.-L. Pan, B. Dai, B. Kiran, J. Li and L.-S. Wang, *J. Phys. Chem. C*, 2008, **112**, 11920-11928.
9. A. Fielicke, G. von Helden, G. Meijer, D. B. Pedersen, B. Simard and D. M. Rayner, *J. Am. Chem. Soc.*, 2005, **127**, 8416-8423.
10. X.-F. Yang, Y.-L. Wang, Y.-F. Zhao, A.-Q. Wang, T. Zhang and J. Li, *Phys. Chem. Chem. Phys.*, 2010, **12**, 3038-3043.
11. F. Furche, R. Ahlrichs, P. Weis, C. Jacob, S. Gilb, T. Bierweiler and M. M. Kappes, *J. Chem. Phys.*, 2002, **117**, 6982-6990.
12. H. Hakkinen, B. Yoon, U. Landman, X. Li, H. J. Zhai and L. S. Wang, *J. Phys. Chem. A*, 2003, **107**, 6168-6175.

13. S. Bulusu, X. Li, L. S. Wang and X. C. Zeng, *Proc. Natl. Acad. Sci.*, 2006, **103**, 8326-8330.
14. B. Yoon, P. Koskinen, B. Huber, O. Kostko, B. von Issendorff, H. Hakkinen, M. Moseler and U. Landman, *Chemphyschem*, 2007, **8**, 157-161.
15. X. P. Xing, B. Yoon, U. Landman and J. H. Parks, *Phys. Rev. B*, 2006, **74**, 165423-1-6.
16. A. Lechtken, C. Neiss, M. M. Kappes and D. Schooss, *Phys. Chem. Chem. Phys.*, 2009, **11**, 4344-4350.
17. M. P. Johansson, A. Lechtken, D. Schooss, M. M. Kappes and F. Furche, *Phys. Rev. A*, 2008, **77**, 053202-1-7.
18. S. Gilb, P. Weis, F. Furche, R. Ahlrichs and M. M. Kappes, *J. Chem. Phys.*, 2002, **116**, 4094-4101.
19. P. Weis, T. Bierweiler, E. Vollmer and M. M. Kappes, *J. Chem. Phys.*, 2002, **117**, 9293-9297.
20. J. R. Soto, B. Molina and J. J. Castro, *Rsc Advances*, 2014, **4**, 8157-8164.
21. B. E. Salisbury, W. T. Wallace and R. L. Whetten, *Chem. Phys.*, 2000, **262**, 131-141.
22. W. T. Wallace and R. L. Whetten, *J. Am. Chem. Soc.*, 2002, **124**, 7499-7505.
23. D. W. Yuan and Z. Zeng, *J. Chem. Phys.*, 2004, **120**, 6574-6584.
24. W. Huang, H. J. Zhai and L. S. Wang, *J. Am. Chem. Soc.*, 2010, **132**, 4344-4351.
25. M. Neumaier, F. Weigend, O. Hampe and M. M. Kappes, *Faraday. Discuss.*, 2008, **138**, 393-406.
26. T. M. Bernhardt, J. Hagen, S. M. Lang, D. M. Popolan, L. D. Socaciu-Siebert and L. Woste, *J. Phys. Chem. A*, 2009, **113**, 2724-2733.
27. J. Hagen, L. D. Socaciu, M. Elijazyfer, U. Heiz, T. M. Bernhardt and L. Woste, *Phys. Chem. Chem. Phys.*, 2002, **4**, 1707-1709.
28. L. D. Socaciu, J. Hagen, T. M. Bernhardt, L. Woste, U. Heiz, H. Hakkinen and U. Landman, *J. Am. Chem. Soc.*, 2003, **125**, 10437-10445.
29. H. Hakkinen and U. Landman, *J. Am. Chem. Soc.*, 2001, **123**, 9704-9705.
30. T. M. Bernhardt, *Int. J. Mass. Spectrom.*, 2005, **243**, 1-29.
31. H. C. Fang, Z. H. Li and K. N. Fan, *Phys. Chem. Chem. Phys.*, 2011, **13**, 13358-13369.
32. Z. Yuan, X.-N. Li and S.-G. He, *J. Phys. Chem. Lett.*, 2014, **5**, 1585-1590.
33. X.-N. Li, Z. Yuan and S.-G. He, *J. Am. Chem. Soc.*, 2014, **136**, 3617-3623.
34. Z.-Y. Li, Z. Yuan, X.-N. Li, Y.-X. Zhao and S.-G. He, *J. Am. Chem. Soc.*, 2014, **136**, 14307-14313.
35. F. Wang, D. J. Zhang, X. H. Xu and Y. Ding, *J. Phys. Chem. C*, 2009, **113**, 18032-18039.
36. A. Prestianni, A. Martorana, F. Labat, I. Ciofini and C. Adamo, *J. Mol. Struc-theochem*, 2009, **903**, 34-40.
37. G. E. Johnson, R. Mitric, V. Bonacic-Koutecky and A. W. Castleman, *Chem. Phys. Lett.*, 2009, **475**, 1-9.
38. M. Boronat and A. Corma, *Dalton. Trans.*, 2010, **39**, 8538-8546.
39. R. C. Deka, D. Bhattacharjee, A. K. Chakrabartty and B. K. Mishra, *Rsc Advances*, 2014, **4**, 5399-5404.
40. Y. Gao, N. Shao, S. Bulusu and X. C. Zeng, *J. Phys. Chem. C*, 2008, **112**, 8234-8238.
41. A. Prestianni, A. Martorana, I. Ciofini, F. Labat and C. Adamo, *J. Phys. Chem. C*, 2008, **112**, 18061-18066.
42. A. Prestianni, A. Martorana, F. Labat, I. Ciofini and C. Adamo, *J. Phys. Chem. B*, 2006, **110**, 12240-12248.
43. B. Yoon, H. Hakkinen, U. Landman, A. S. Worz, J. M. Antonietti, S. Abbet, K. Judai and U. Heiz, *Science*, 2005, **307**, 403-407.
44. S. A. Serapian, M. J. Bearpark and F. Bresme, *Nanoscale*, 2013, **5**, 6445-6457.
45. M. Neumaier, F. Weigend, O. Hampe and M. M. Kappes, *J. Chem. Phys.*, 2005, **122**, 104702-1-11.
46. D. M. Popolan, M. Nossler, R. Mitric, T. M. Bernhardt and V. Bonacic-Koutecky, *Phys. Chem. Chem. Phys.*, 2010, **12**, 7865-7873.
47. P. Schwerdtfeger, M. Lein, R. P. Krawczyk and C. R. Jacob, *J. Chem. Phys.*, 2008, **128**, 124302-1-10.
48. X. Wu, L. Senapati, S. K. Nayak, A. Selloni and M. Hajaligol, *J. Chem. Phys.*, 2002, **117**, 4010-4015.
49. A. S. Worz, U. Heiz, F. Cinquini and G. Pacchioni, *J. Phys. Chem. B*, 2005, **109**, 18418-18426.
50. F. Menegazzo, M. Manzoli, A. Chiorino, F. Boccuzzi, T. Tabakova, M. Signoretto, F. Pinna and N. Pernicone, *J. Catal.*, 2006, **237**, 431-434.
51. L. Jiang and Q. Xu, *J. Phys. Chem. A*, 2005, **109**, 1026-1032.
52. M. J. Frisch, G. W. Trucks, H. B. Schlegel and Etal., *Gaussian 09, Revision A02, Gaussian, Inc., Wallingford, CT*, 2009.
53. *http://sourceforge.net/projects/atomicglobalmin/*.
54. B. B. Averkiev, S. Call, A. I. Boldyrev, L.-M. Wang, W. Huang and L.-S. Wang, *J. Phys. Chem. A*, 2008, **112**, 1873-1879.
55. S. T. Call, D. Y. Zubarev and A. I. Boldyrev, *J. Comput. Chem.*, 2007, **28**, 1177-1186.
56. J. Clark, S. T. Call, D. E. Austin and J. C. Hansen, *J. Phys. Chem. A*, 2010, **114**, 6534-6541.
57. C. Lee, W. Yang and R. G. Parr, *Phys. Rev. B*, 1988, **37**, 785-789.
58. A. D. Becke, *J. chem. phys.*, 1993, **98**, 1372-1377.
59. M. Neumaier, F. Weigend, O. Hampe and M. M. Kappes, *J. Chem. Phys.*, 2006, **125**, 104308-1-10.
60. Q. Xu and L. Jiang, *J. Phys. Chem. A*, 2006, **110**, 2655-2662.
61. A. Martinez, *J. Phys. Chem. C*, 2010, **114**, 21240-21246.
62. H.-C. Fang, Z. H. Li and K.-N. Fan, *Phys. Chem. Chem. Phys.*, 2011, **13**, 13358-13369.
63. P. V. Nhat, T. B. Tai and M. T. Nguyen, *J. Chem. Phys.*, 2012, **137**, 164312-1-12.
64. S. Rai, N. V. S. Kumar and H. Singh, *B. Mater. Sci.*, 2012, **35**, 291-295.
65. Z. Jamshidi, H. Farhangian and Z. A. Tehrani, *Int. J. Quantum Chem.*, 2013, **113**, 1062-1070.
66. H. Hakkinen and U. Landman, *Phys. Rev. B*, 2000, **62**, 2287-2290.
67. K. A. Peterson and C. Puzzarini, *Theo. Chem. Acc.*, 2005, **114**, 283-296.
68. D. Figgen, G. Rauhut, M. Dolg and H. Stoll, *Chem. Phys.*, 2005, **311**, 227-244.
69. T. H. Dunning, *J. Chem. Phys.*, 1989, **90**, 1007-1023.
70. R. A. Kendall, T. H. Dunning and R. J. Harrison, *J. Chem. Phys.*, 1992, **96**, 6796-6806.
71. J. Velasquez, B. Njegic, M. S. Gordon and M. A. Duncan, *J. Phys. Chem. A*, 2008, **112**, 1907-1913.
72. A. Deka, R. C. Deka and A. Choudhury, *Chem. Phys. Lett.*, 2010, **490**, 184-188.

Fig. 1

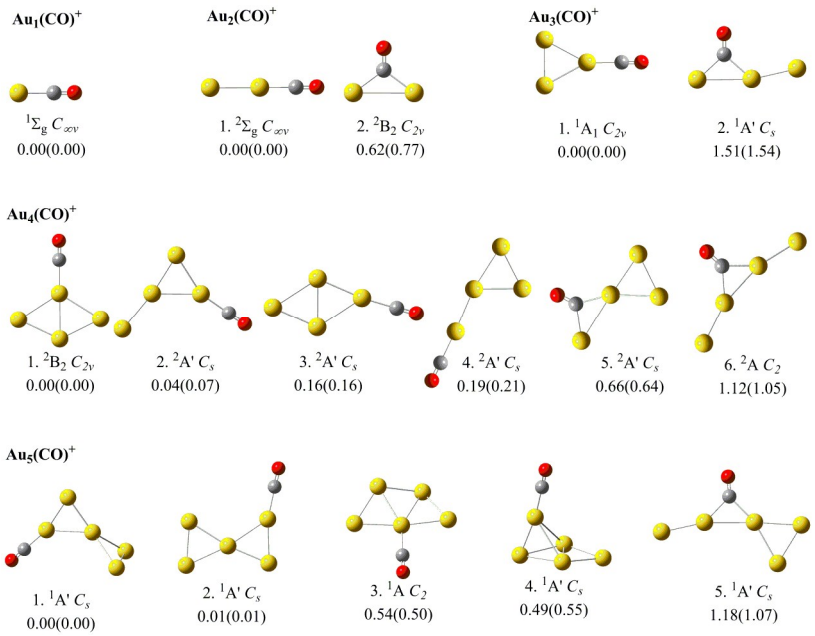

Fig. 2

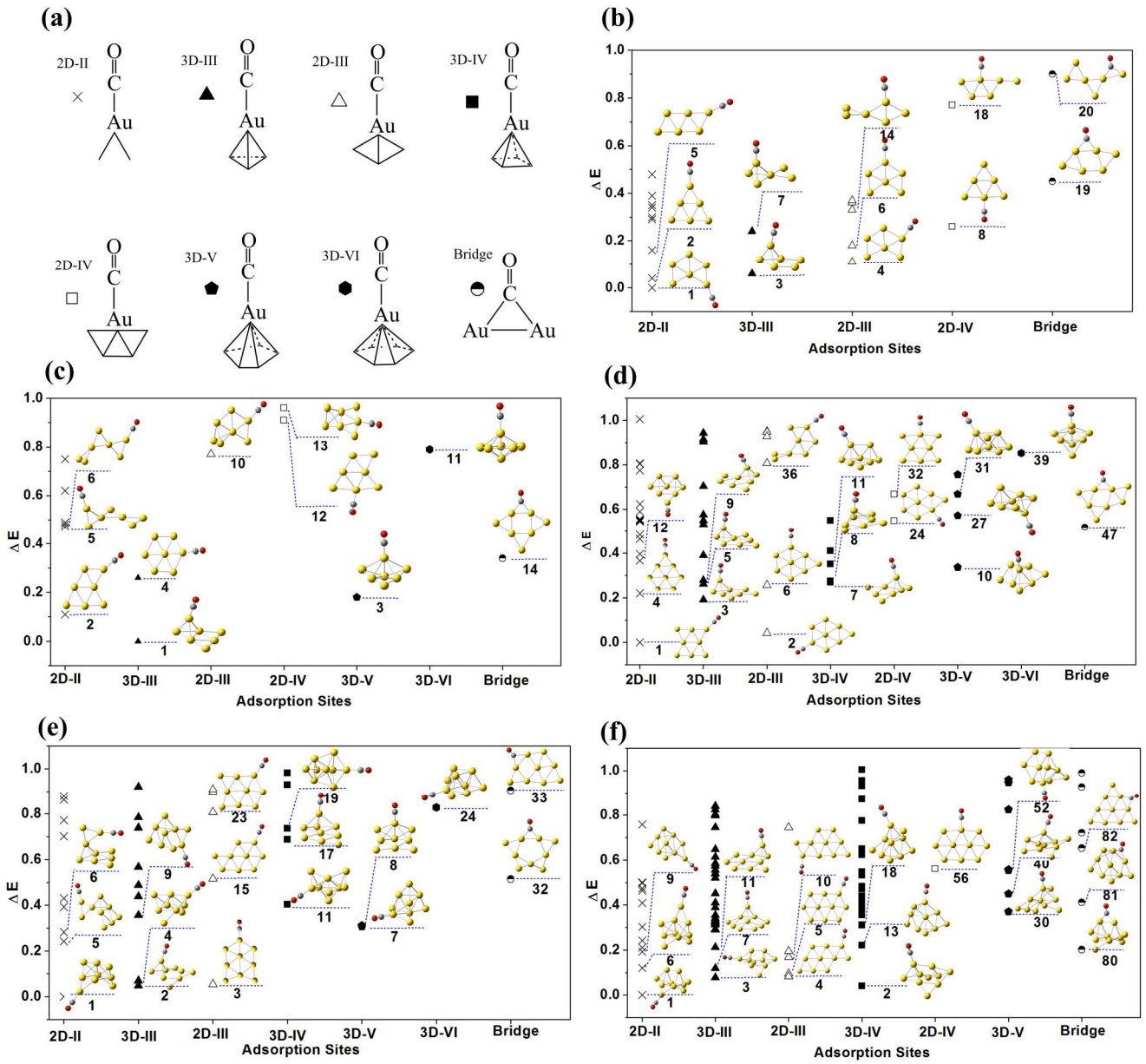

Fig. 3

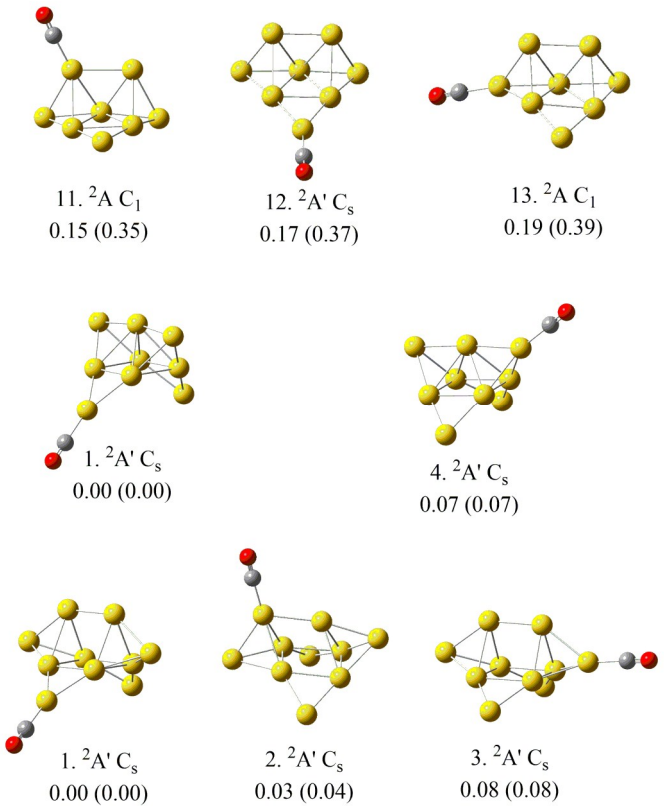

Fig. 4

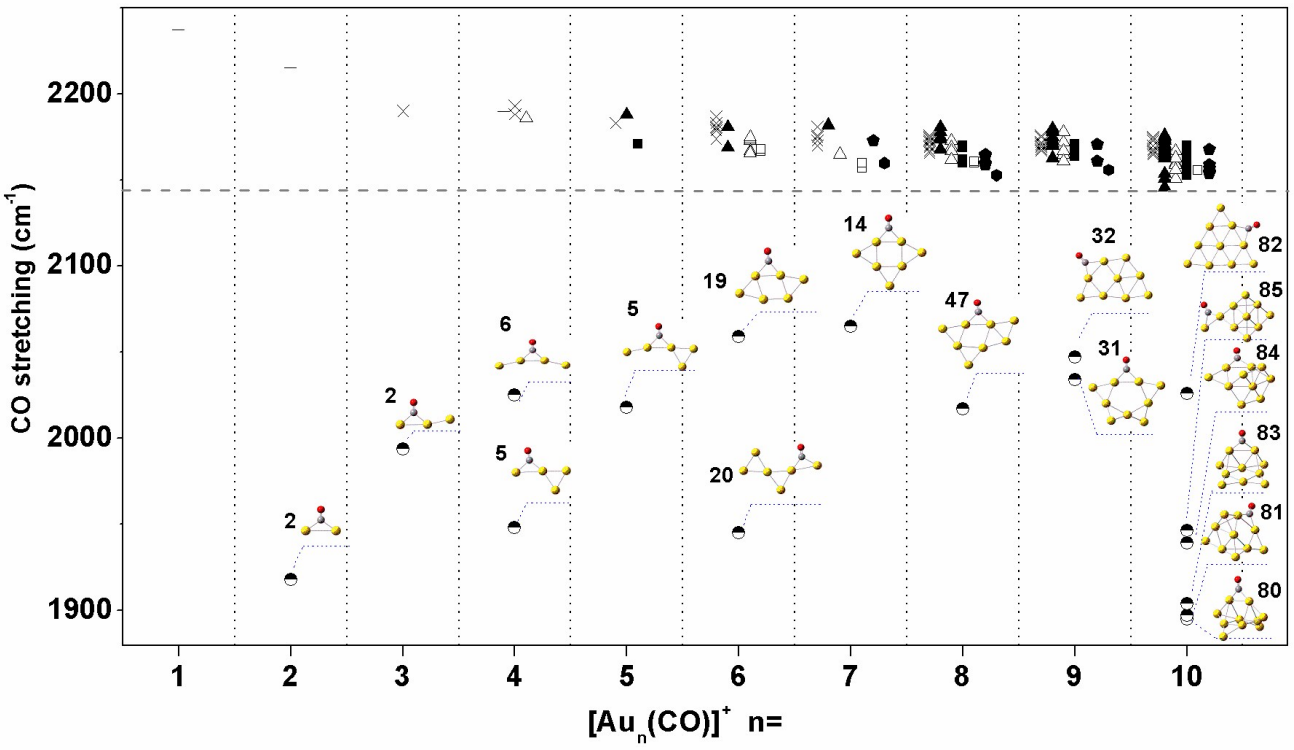

Fig. 5

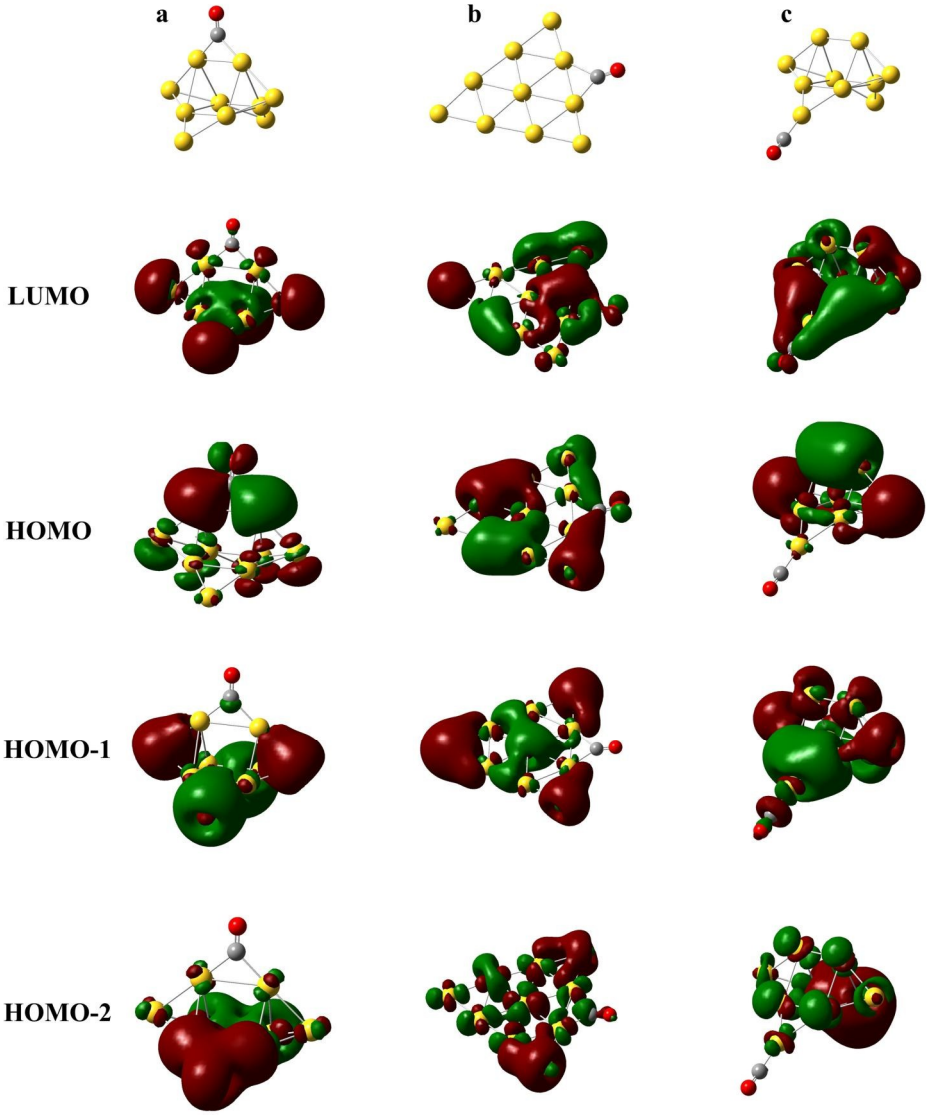

Adsorption of CO on cationic gold clusters is insensitive to the structural details of the adsorption site.

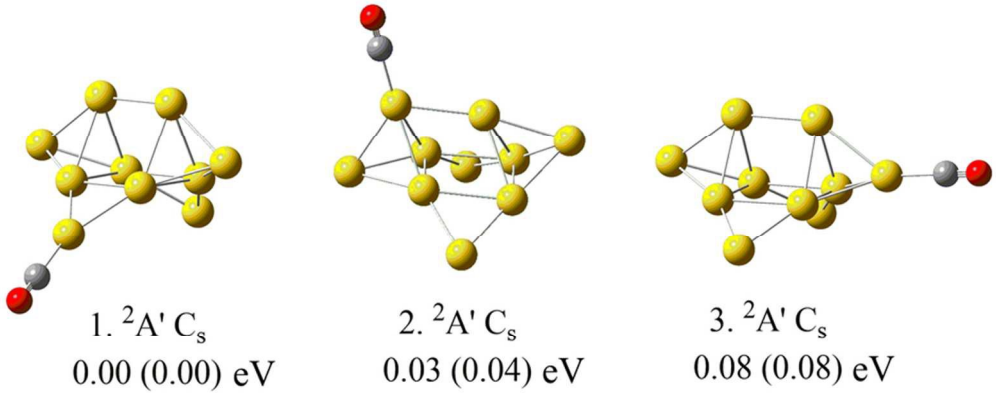

40x20mm (600 x 600 DPI)